**PAPER**

# Estimating petrophysical reservoir properties through extended elastic impedance inversion: applications to off-shore and on-shore reflection seismic data

IOP Publishing Journal of Geophysics and Engineering
J. Geophys. Eng. **15** (2018) 2079–2090 (12pp) https://doi.org/10.1088/1742-2140/aac54b

# Estimating petrophysical reservoir properties through extended elastic impedance inversion: applications to off-shore and on-shore reflection seismic data

**Mattia Aleardi**

University of Pisa, Earth Sciences Department, Italy

E-mail: mattia.aleardi@dst.unipi.it

Received 25 January 2018, revised 18 March 2018
Accepted for publication 16 May 2018
Published 21 June 2018

**Abstract**

We use an extended elastic impedance (EEI) inversion for quantitative reservoir characterization. The EEI approach is applied to both on-shore and off-shore seismic data where target reservoirs are gas-bearing sands located in sand-shale sequences. The workflow we adopt can be divided into three phases. The starting point is a petrophysical analysis in which the relationships between petrophysical and elastic properties are analyzed. The second step of EEI analysis uses a cross-correlation procedure to determine the best chi ($\chi$) projection angles for the petrophysical parameters of interest (i.e. porosity, water saturation and shaliness). In the final step, pre-stack seismic data are simultaneously inverted into *P*-wave velocity, acoustic, and gradient impedances, and the last two elastic volumes are finally projected to $\chi$ angles corresponding to the target petrophysical parameters. The estimated porosity, water saturation, and shaliness values reveal a proper match at blind well locations. This work shows that EEI is an effective tool for lithology and fluid prediction in clastic reservoirs. The output of this work can be beneficial for static reservoir model building and volumetric calculation and can be also used to determine new potential drilling locations.

Keywords: reservoir characterization, amplitude inversion, extended elastic impedance

(Some figures may appear in colour only in the online journal)

## Introduction

A robust estimation of petrophysical parameters such as shaliness (Sh), water saturation (Sw), and porosity ($\varphi$) around the investigated reservoir zone is of utmost importance mainly for three objectives: static geological model building, volumetric reserve estimation, and overall field development planning. Many studies in the literature discuss the transformation of band-limited seismic data into reservoir properties. One of the most common inversion approaches consists of first inverting seismic data into elastic parameters, and then converting the estimated elastic attributes into petrophysical reservoir properties through a rock-physics model or statistical relationships between the petrophysical and elastic parameters derived at well control points (Dubucq *et al* 2001, Vernik *et al* 2002, Avseth *et al* 2010, Chatterjee *et al* 2013, Aleardi and Ciabarri 2017a, Aleardi 2018). However, to deal with the ill-posedness of such seismic-petrophysical inversion, regularization strategies are usually introduced into the inversion kernel (Doyen 1988, Bachrach 2006, Sengupta and Bachrach 2007, Grana and Della Rossa, 2010, Sams *et al* 2011, Aleardi and Ciabarri 2017b, Aleardi *et al* 2017).

In addition to the seismic-petrophysical inversion, the extended elastic impedance (EEI; Whitcombe *et al* 2002) inversion has also been established as a key technology solution for lithology and fluid prediction in the exploration and production industry (Shi *et al* 2014, Samba *et al* 2017). This technology started with Connolly (1999), who, basing it on linearization of the Zoeppritz equations, defined the elastic impedance (EI) as the equivalent of acoustic impedance (AI)

 

at non-zero angles. This opened a new dimension of utilization of AI–EI pairs for lithology and fluid discrimination. While Connolly's work provides good results and useful guides for enhanced reservoir characterization, restriction of incident angles was a serious challenge. An additional problem is that EI has strange unit and dimensions and its values do not scale correctly for different angles. This last EI limitation was overcome by Whitcombe *et al* (2002) who modified the Connolly formula by introducing three normalizing constants which represent average values of velocities and densities over the zone of interest. These normalizing constants remove the variable dimensionality and provide the EI with the same dimensionality and scale of AI. Whitcombe *et al* (2002) further introduced the EEI approach to overcome the limitation concerning the incidence angles. In fact, he broadened the definition of EI to remove the dependence of its dimensionality on the incidence angle. He recognized that some rock properties cannot be predicted from existing seismic gathers due to limitation on the incidence angle range (usually 0°–30°). That is to say, the squared sinus of the incidence angle ($\theta$) needs to exceed unity to make the estimation of key petrophysical properties possible. To solve this problem Whitcombe *et al* (2002) introduced the EEI concept by substituting the squared sinus of the incidence angle with the tangent of chi ($\chi$), with $\chi$ varying between $-90°$ and 90°. In the context of reservoir characterization, it has been demonstrated that the EEI at optimized $\chi$ angles correlates well with elastic and reservoir properties.

The key step of the EEI method is to use a data-driven approach to determine the best projection $\chi$ angles for target well logs representing sought parameters. The target logs can be given elastic properties (i.e. $Vp/Vs$ ratio, bulk modulus, Lamé constants, seismic-impedances) or petrophysical rock properties (i.e. porosity, water saturation, shaliness). To determine the best $\chi$ angles, the EEI log spectrum can be used. This method first generates the EEI log spectrum by making use of logged velocity and density values and then cross-correlates the obtained EEI spectrum at different $\chi$ angles with the sought parameters in order to give an estimate of the optimum angles to use. Depending on the quality of well log data, one can expect to see a perfect correlation between the EEI log and reservoir properties such as porosity, clay content, and water saturation. It is worth stating that factors like depth trend (Ball *et al* 2013, 2014, Thomas *et al* 2013), compaction trend (Avseth *et al* 2013), thickness, and lithology influence the quality of the correlation. Recently, Thomas *et al* (2013) have recommended the use of the natural logarithm of EEI (ln EEI) instead of the full EEI during the correlation analysis between reservoir properties and EEI logs to avoid statistical biases and loss of parity with reflection. Once the best projection angles have been estimated for the rock properties we are interested in, a pre-stack seismic inversion can be performed to infer the EEI values away from well locations. Then, the inverted EEI volumes can be projected onto the subsurface properties of interest by exploiting the optimal $\chi$ angles.

This paper is mainly aimed at illustrating the reliability and the suitability of the EEI method for reservoir characterization in clastic reservoirs located in shale-sand sequences. In particular, we use the concept of EEI to derive three petrophysical properties (porosity, water saturation and shaliness) for two different gas-saturated reservoirs. We use the estimated optimal $\chi$ angles to convert the inverted acoustic and gradient impedance (GI) cubes into the petrophysical properties of interest. The first part of the paper discusses the theory behind the EEI method and describes the inversion approach we use. In the second part, the methodology is applied to two seismic datasets acquired on-shore and off-shore.

## The method

Whitcombe *et al* (2002) defined the EEI as follows:

$$\mathrm{EEI}(\chi) = Vp_0\rho_0\left[\left(\frac{Vp}{Vp_0}\right)^{\cos\chi+\sin\chi}\left(\frac{Vs}{Vs_0}\right)^{-8K\sin^2(\chi)} \times\left(\frac{\rho}{\rho_0}\right)^{\cos\chi-4K\sin\chi}\right], \quad (1)$$

where $\rho$ is the density, $\rho_0$, $Vp_0$ and $Vs_0$ are normalizing constants for $Vp$, $Vs$ and density, respectively, and $K$ is the average squared $Vs/Vp$ ratio over the target depth interval. Obtaining EEI reflectivity volumes at $\chi = 0$ and $\chi = 90$ degrees so that they can be transformed into AI and GI, respectively, was one of the reasons leading to the development of the EEI approach. To this aim, equation (1) can be also rewritten as follows:

$$\mathrm{EEI}(\chi) = \mathrm{AI}_0\left(\frac{\mathrm{AI}}{\mathrm{AI}_0}\right)^{\cos\chi}\left(\frac{\mathrm{GI}}{\mathrm{AI}_0}\right)^{\sin\chi}, \quad (2)$$

where $\mathrm{AI}_0$ is the normalization factor for AI. If we consider the two term Shuey approximation to the Zoeppritz equations (Shuey 1985), $\chi$ can be considered as the rotational angle in the intercept-gradient plane that is related to the angle of incidence $\theta$ as follows:

$$\tan\chi = \sin^2\theta. \quad (3)$$

It can be noted that equation (3) extends the range of measured data imposed by $\sin^2\theta$ ($0 < \sin^2\theta < 1$) to minus and plus infinities.

From the previous equations it emerges that the AI and GI values are needed to infer the EEI values for different $\chi$ angles away from well locations. The AI and GI values can be estimated through a pre-stack inversion of seismic data. To this end we implement a simultaneous inversion that is a modification of the amplitude versus angle (AVA) inversion algorithm proposed by Hampson *et al* (2005).

By convolving the AVA equation given by Wiggins *et al* (1983) with the angle-dependent source wavelet $W(\theta)$, the synthetic seismic trace for a given incidence angle can be

defined as:

$$Spp(\theta) = \frac{a}{2}W(\theta)\Delta \ln(\mathrm{AI}) + \frac{b}{2}W(\theta)\Delta\delta \ln(\mathrm{GI}) + \frac{c}{2}W(\theta)\Delta\delta \ln(Vp), \quad (4)$$

where $\Delta$ expresses the sample-by-sample contrasts, $\delta$ are the deviations from a linear trend (see below), whereas the numerical coefficients $a$, $b$ and $c$ are defined by:

$$a = 1 + \alpha_{\mathrm{GI}} b + \alpha_{Vp} c\,, \quad (5.1)$$

$$b = \sin^2(\theta)\,, \quad (5.2)$$

$$c = \sin^2(\theta)\tan^2(\theta). \quad (5.3)$$

In equation (5.1) $\alpha_{\mathrm{GI}}$ is the gradient coefficient of the linear equation ln(GI) versus ln(AI):

$$\ln(\mathrm{GI}) = \alpha_{\mathrm{GI}} \ln(\mathrm{AI}) + k_{\mathrm{GI}} + \delta \ln(\mathrm{GI}), \quad (6)$$

where $k_{\mathrm{GI}}$ is the intercept term and the $\delta$ln(GI) term defines the deviations away from the linear equation (6). Similarly, in equation (5.1) $\alpha_{Vp}$ is the gradient coefficient of the linear equation ln($Vp$) versus ln(AI):

$$\ln(Vp) = \alpha_{Vp} \ln(\mathrm{AI}) + k_{Vp} + \delta \ln(Vp), \quad (7)$$

where $k_{Vp}$ is the intercept term and $\delta$ln($Vp$) defines the deviations away from the linear equation (7). Equations (6) and (7) can be defined making use of an optimization procedure driven by available well log data. Note from equation (4) that we are mainly looking for deviations away from a linear fit in natural logarithmic space.

In matrix notation, the linear forward modeling of equation (4) can be written as follows:

$$\begin{bmatrix} Spp(\theta_1) \\ Spp(\theta_2) \\ \vdots \\ Spp(\theta_N) \end{bmatrix} = \begin{bmatrix} \frac{a(\theta_1)}{2}W(\theta_1)D & \frac{b(\theta_1)}{2}W(\theta_1)D & \frac{c(\theta_1)}{2}W(\theta_1)D \\ \frac{a(\theta_2)}{2}W(\theta_2)D & \frac{b(\theta_2)}{2}W(\theta_2)D & \frac{c(\theta_2)}{2}W(\theta_2)D \\ \vdots & \vdots & \vdots \\ \frac{a(\theta_N)}{2}W(\theta_N)D & \frac{b(\theta_N)}{2}W(\theta_N)D & \frac{c(\theta_N)}{2}W(\theta_N)D \end{bmatrix} \begin{bmatrix} \ln(\mathrm{AI}) \\ \delta \ln(\mathrm{GI}) \\ \delta \ln(Vp) \end{bmatrix}, \quad (8)$$

where $N$ is the total number of incidence angles we consider, and $D$ is the numerical differential operator; $W$ is a banded matrix composed of extracted wavelets per partial angle stack, whereas $Spp$ is the data column vector containing samples of partial angle stack for each considered incidence angle.

In particular, in our implementation we stabilize the inversion procedure by adding *a priori* information about the mutual correlation and the vertical variability of the considered elastic properties. This *a priori* information can be derived from available well log data. More in detail, equation (8) can be written as follows:

$$\mathbf{d} = \mathbf{G}\mathbf{m}, \quad (9)$$

where $\mathbf{d}$ represents the observed data vector, $\mathbf{G}$ is the linear forward model and $\mathbf{m}$ is the model vector. In solving

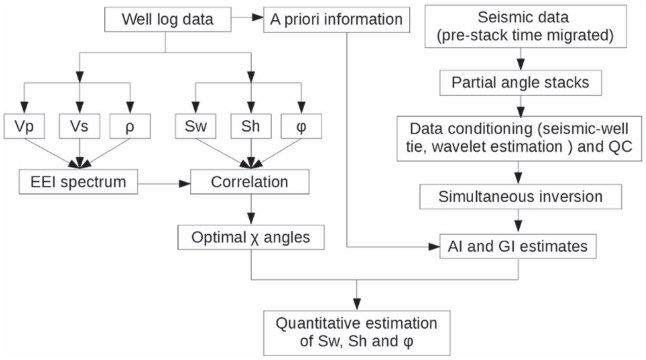


**Figure 1.** Schematic representation of the workflow of the methodology.

equation (8) we minimize the following error function:

$$E(\mathbf{m}) = \|\mathbf{C}_{\mathbf{d}}^{-1/2}(\mathbf{d} - \mathbf{G}\mathbf{m})\|_2^2 + \|\mathbf{C}_{\mathbf{m}}^{-1/2}(\mathbf{m} - \mathbf{m}_{\mathbf{prior}})\|_2^2, \quad (10)$$

where $\mathbf{m}_{\mathbf{prior}}$ is the prior model, $\mathbf{C}_{\mathbf{d}}$ is the data covariance matrix describing the noise affecting the observed data, and $\mathbf{C}_{\mathbf{m}}$ is the *a priori* model covariance matrix expressing both the mutual correlation of elastic properties and their vertical variability. The matrix $\mathbf{C}_{\mathbf{m}}$ can be obtained by a Kronecker product between a stationary correlation matrix expressing the mutual correlation of elastic properties and a vertical correlation function coding the vertical variability of elastic properties. In particular, following Buland and Omre (2003) such vertical correlation can be expressed by a second-order exponential function that approximates the actual vertical variability of elastic properties.

Under the assumption of Gaussian statistic, the least-square solution of equation (10), can be derived as follows:

$$\mathbf{m} = [\mathbf{G}^{\mathbf{T}}\mathbf{C}_{\mathbf{d}}^{-1}\mathbf{G} + \mathbf{C}_{\mathbf{m}}^{-1}]^{-1}[\mathbf{G}^{\mathbf{T}}\mathbf{C}_{\mathbf{d}}^{-1}\mathbf{d} + \mathbf{C}_{\mathbf{m}}^{-1}\mathbf{m}_{\mathbf{prior}}]. \quad (11)$$

For computational feasibility reasons, we solve equation (11) iteratively (i.e. employing the conjugate gradient method) by starting the inversion from an initial model and then iterate toward the final solution until the desired data-misfit value is attained. We invert each seismic gather separately, thus overlooking the spatial correlation of elastic attributes. However, we point out that the lateral continuity of our results is imposed by the lateral correlation of seismic data that depends on the migration operator.

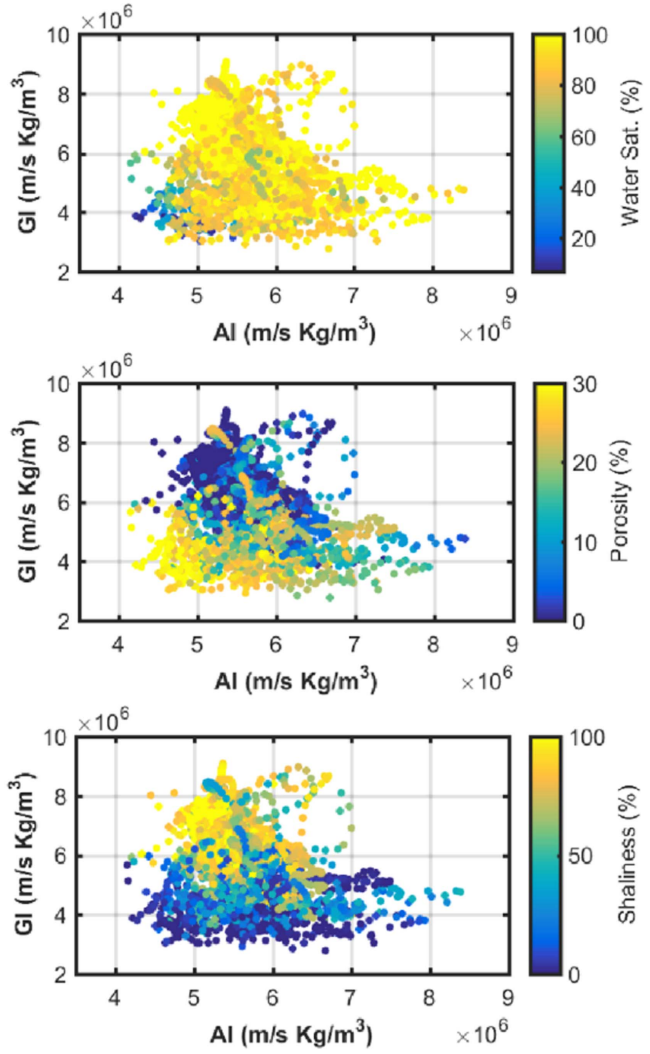


**Figure 2.** Rock-physics templates showing the influence of each petrophysical parameter on the acoustic impedance (AI) and gradient impedance (GI). The influences of water saturation, porosity and shaliness are represented from top to bottom.

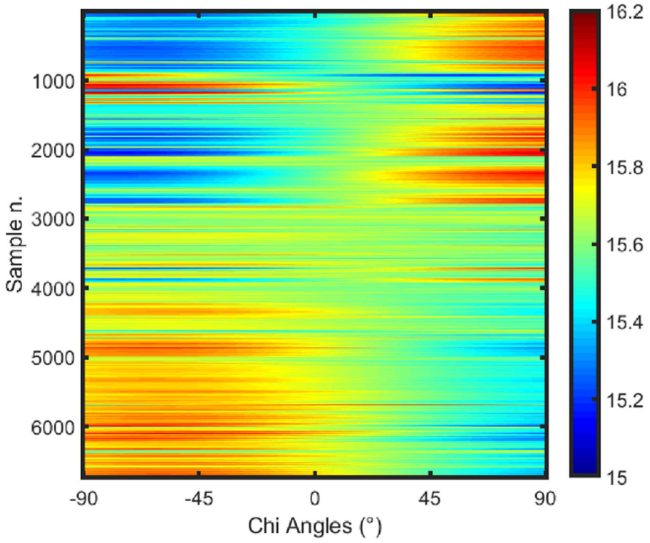


**Figure 3.** Example of EEI log spectrum obtained by applying equation (1) to logged *Vp*, *Vs* and density values.

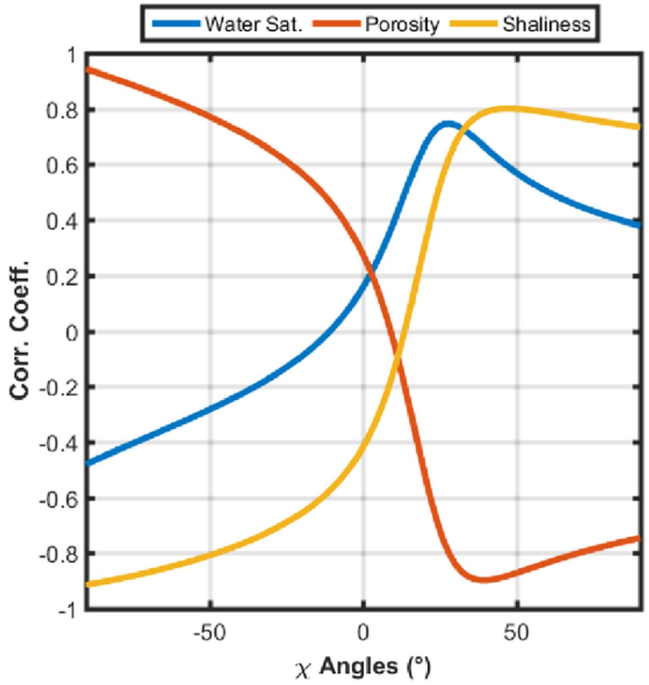


**Figure 4.** Cross-correlation analysis for the investigated reservoir located off-shore.

## Field case applications

We now describe the results obtained in two applications of the EEI method for reservoir characterization on on-shore and off-shore data. In both cases the targets of the investigation are gas-saturated clastic reservoirs located in shale-sand sequences. Figure 1 shows the workflow of the methodology used in this study. It starts from well log data, previously analyzed and quality controlled to ensure that the required data are available and physically reasonable. Then, we compute the EEI logs for different $\chi$ angles using equations (1) or (2) and we estimate the optimum angles that give the best correlation (positive or negative) between the EEI and the petrophysical target logs (porosity, shaliness, and water saturation). Then, we perform a quality control, conditioning and simultaneous inversion of pre-stack time-migrated data with the aim to estimate *P*-wave velocity, acoustic, and GIs. In this inversion, *a priori* information derived from available well log data are included to attenuate the ill-conditioning of the inverse problem. We compute the equivalent EEI volume through equation (2) and we finally transform such EEI volume into quantitative petrophysical properties.

Determining the optimum $\chi$ angle for a target reservoir property is the primary base to a successful application of the proposed technique. Hence, high quality well log data are needed for the computation of EEI as well as for the correlation analysis. A set of EEI logs ranging from $\chi = -90°$ to $\chi = 90°$ was then computed by means of equation (1). The normalization constants have been estimated by averaging logged velocity and density values around the target interval. In the computation of the optimal $\chi$ angles we follow the guidelines proposed by Thomas *et al* (2013). They suggested performing an accurate

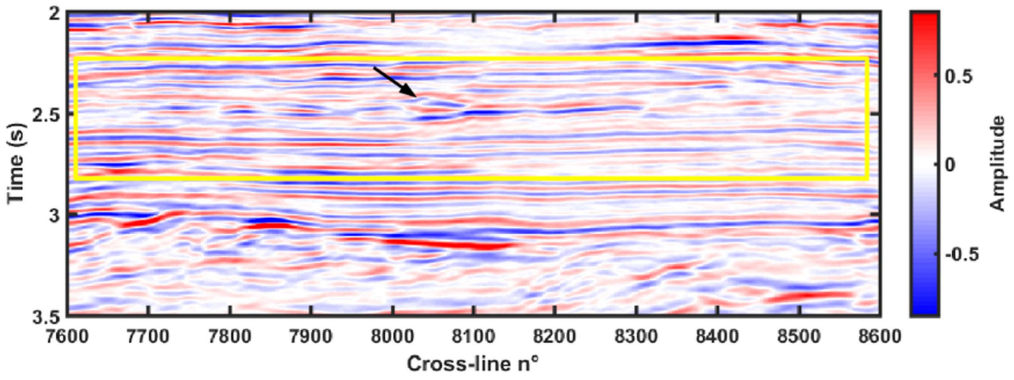


**Figure 5.** Example of stack section along an in-line direction extracted from the 3D seismic volume. The yellow rectangle delimits the target zone, while the black arrow points toward the top reflection of the reservoir layer.

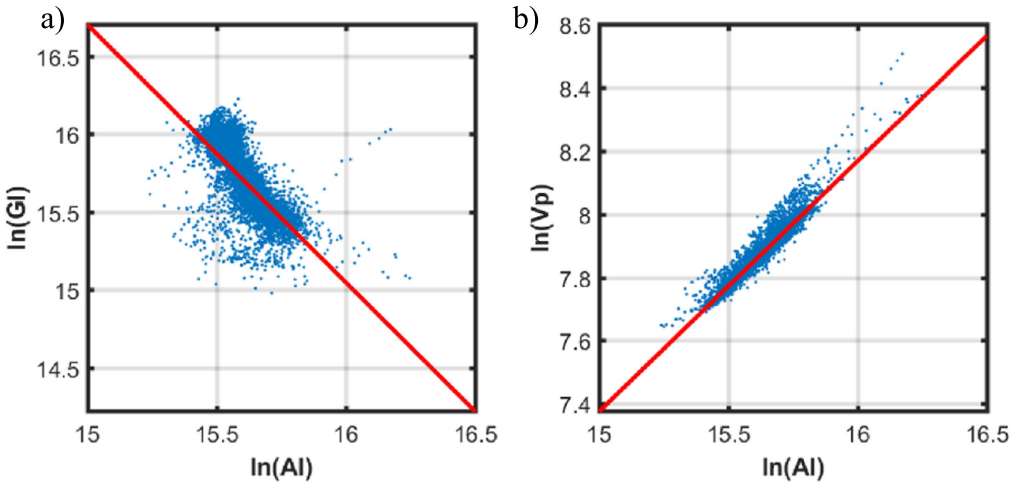


**Figure 6.** Cross-plots of ln(AI) versus ln(GI) (part (a)) and ln(AI) versus ln($Vp$) (part (b)), together with the resulting linear fits. Blue dots represent well log samples, while the red lines show the estimated linear regressions.

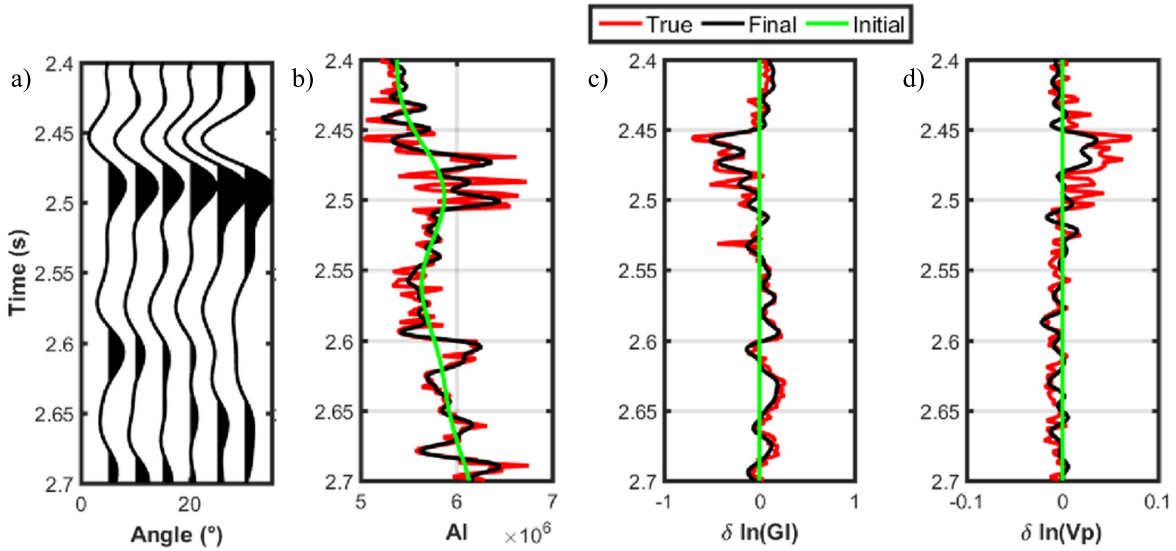


**Figure 7.** Inversion results for the seismic gather closest to the blind well. (a)–(d) Represent the seismic data, the acoustic impedance, the $\delta$ln (GI) and the $\delta$ln($Vp$), respectively. In (b)–(d) the red, green and black lines show the true, the initial, and the final predicted models, respectively. The amplitude anomaly at 2.45 s identifies the reservoir reflection.

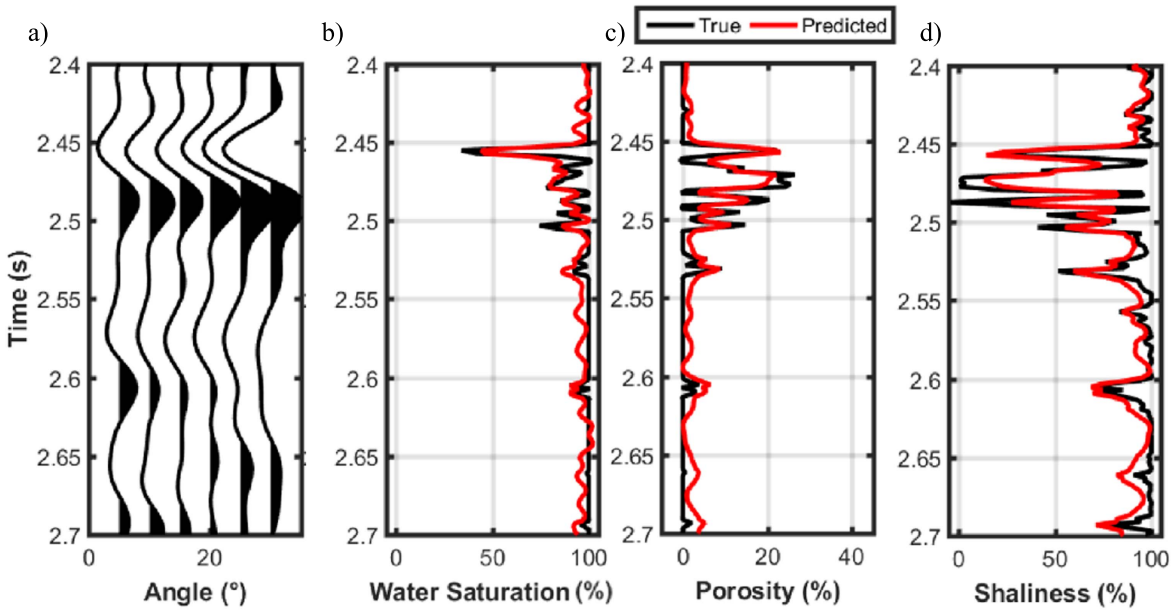


**Figure 8.** Petrophysical properties estimated for the seismic gather closest to the blind well. (a)–(d) Represent the seismic data, water saturation, porosity and shaliness, respectively. In (b)–(d) the black and red lines represent the true and the final predicted models, respectively. As in figure 7(a), the amplitude anomaly at 2.45 s identifies the reservoir reflection.

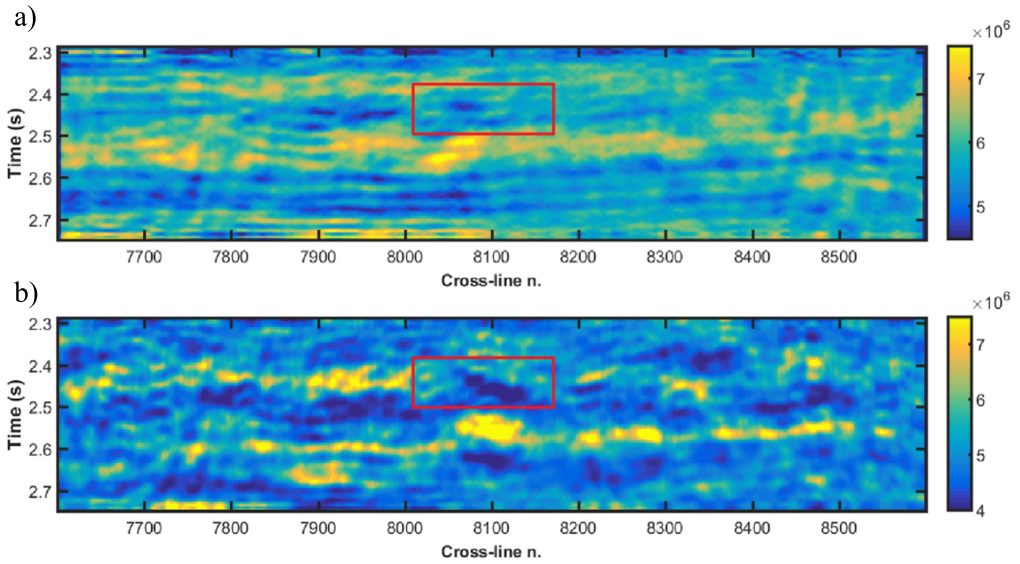


**Figure 9.** (a) and (b) Show the AI and GI values estimated within the yellow rectangle represented in figure 5. The red rectangles enclose the target reservoir characterized by low AI and GI values.

outlier removal procedure from well log data, the use of the natural logarithm of EEI in the correlation analysis instead of full EEI, and the use of the detrended target petrophysical curves and detrended ln(EEI) curves when performing the correlation analysis. Indeed, well logs are generally trended, and the trends associated with ln(EEI) logs are function of the $\chi$ angle. It is well documented that spurious correlation coefficients may result by correlating two trended data (Ball *et al* 2013, 2014). Following Ball *et al* (2014), each single ln(EEI) curve and the petrophysical target log were decomposed into the background trend and the relative components before determining the optimum angle. The correlation analysis is then carried out between the two relative components.

Depending on the quality of the well log data, the correlation coefficient versus $\chi$ angle may show a maximum/minimum peak or a plateau. In case of a plateau, one of the values along the plateau or its center could be considered to be optimal (Thomas *et al* 2013). Once the correlation between the target log and ln(EEI) logs for each $\chi$ angle was obtained, the maximum (positive) or minimum (negative) correlation was identified together with the corresponding $\chi$ angle. This procedure identifies the optimal angle for a given target log, while the correlation value indicates the reliability with which a given petrophysical property can be predicted.

After the cross-correlation analysis, quality control and conditioning of available seismic data is performed with the

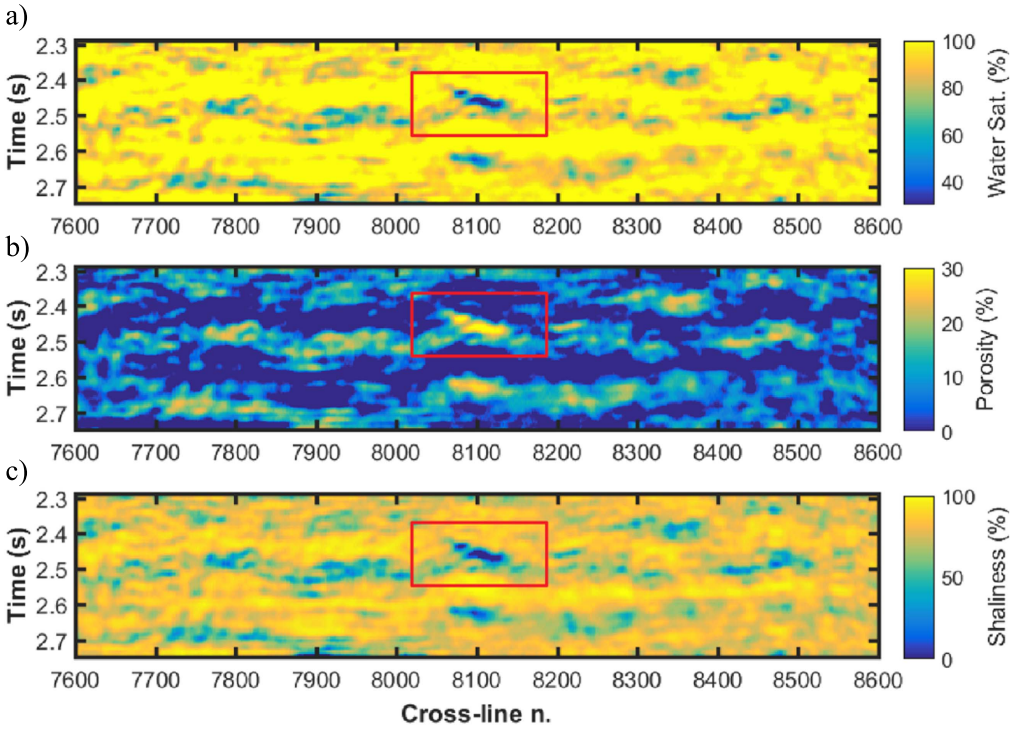


**Figure 10.** Petrophysical properties estimated within the yellow rectangle represented in figure 5. (a)–(c) Refer to water saturation, porosity and shaliness, respectively. The red rectangles enclose the investigated reservoir characterized by high porosity and low water saturation and shaliness values.

aim to detect and fix potentials problems and thus prepare the seismic data for quantitative AVA studies. Accurate amplitude-preserving processing, seismic-well tie, events alignment for optimal AVA response, zero-phase deconvolution, and pre-stack time-migration, have been performed before inversion. Individual wavelets estimated from well-to-seismic tie were used in zero phasing to match the spectral component with reference angle stack. If needed, amplitude balancing, band pass filter and offset dependent scaling could be applied to maintain consistency between well and seismic AVA responses.

For what concerns the inversion approach we apply a deterministic inversion based on equations (8), (10), and (11). In this type of inversion, an initial AI model is modified iteratively to improve its fit with the observed seismic data. To define the initial impedance model available well log data have been used.

## Field case 1: reservoir characterization on off-shore seismic data

In this investigated field, the targets are gas-bearing sands at the depth range of 2300–2700 m. Layering is typically on the centimeter scale, and the reservoir mainly consists in rather clean-sand layers interbedded with laminated non-permeable shales, whereas in localized portions the sand bodies are characterized by a negligible amount of limestone and anhydrite. Eleven out of twelve wells drilled through the target interval, provide elastic and petrophysical properties needed to determine the optimal $\chi$ angles and to define the *a priori* information to be inserted into the inversion kernel. The remaining well has been used as a blind test to check the reliability of our results and to determine the prediction capability of the method for the investigated reservoir. Additional information about the petrophysical characteristics of this area can be found in Aleardi and Ciabarri (2017a).

We first analyze the rock-physics template showing the influence of each petrophysical property of interest on the AI and GI values (figure 2). As expected, we observe a decrease of AI and GI as the water saturation and shaliness decrease and as the porosity increases.

Figure 3 shows an example of EEI log spectrum obtained by applying equation (1) to the logged elastic properties extracted from available well log data. In the following step, we perform a correlation analysis in which the EEI curve obtained for each $\chi$ angle is correlated with each sough petrophysical parameter. This gives the EEI angle correlation curves shown in figure 4.

For a $\chi$ angle equal to $-90$, the porosity shows a very strong positive correlation with ln(EEI), whereas for the same angle the shaliness shows a strong negative correlation coefficient. These characteristics evidence the cross-talk, or in other words the negative correlation, between porosity and shaliness. Differently water saturation gives the highest correlation with ln(EEI) for a $\chi$ angle equal to 27°. Therefore, the EEI log at $\chi = -90$ is an extremely good predictor for both porosity and shaliness, whereas the EEI log at $\chi = 27$ offers a satisfactory prediction of water saturation.

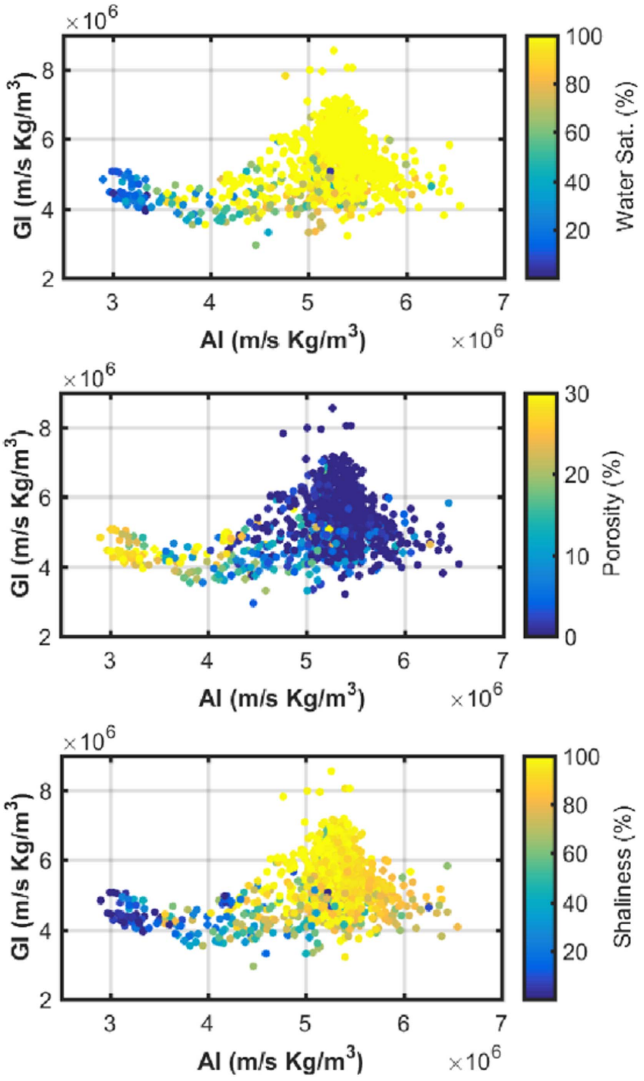


**Figure 11.** Rock-physic templates showing the influence of each petrophysical parameter on the acoustic impedance (AI) and gradient impedance (GI). The influences of water saturation, porosity and shaliness are represented from top to bottom.

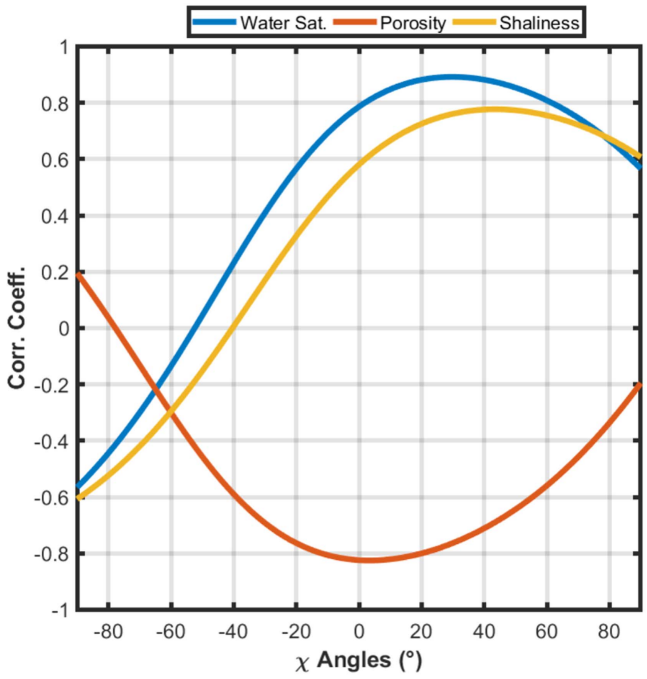


**Figure 12.** Cross-correlation analysis for the investigated reservoir located on-shore.

Figure 5 shows an in-line section extracted from the 3D seismic volume. The yellow rectangle encloses the area that will be considered in the following inversion, whereas the black arrow points to the top reflection of the target reservoir layer. Note the strong amplitude anomaly marking the transition from the cap-rock shale to the reservoir, gas-saturated, sand.

As an example, figure 6 illustrates cross-plots derived from well log data of ln(AI) versus ln(GI) and ln(AI) versus ln($Vp$), together with the resulting linear least-squares fits (see equations (6) and (7)). The slopes of the red lines shown in figures 6(a) and (b) have been used to derive the numerical coefficients $\alpha_{GI}$ and $\alpha_{Vp}$ in equation (5.1), respectively. In this work we are limited to a linear inversion and for this reason we are forced to perform a linear fitting in the ln(AI)–ln(GI) and ln(AI)–ln($Vp$) planes. Other more accurate nonlinear fitting procedures will make the forward modeling not linear, thus increasing the computational cost of the inversion procedure. However, note that the accuracy of the fitting is not a major issue in our case. Indeed, we define (assume) linear relations between ln(AI)–ln(GI) and ln(AI)–ln($Vp$) and, then we invert to infer the deviations from such linear trends. This peculiar parameterization (in terms of deviations from assumed linear trends) is able to provide accurate predictions even if the linear equations do not fully describe the relations between the considered elastic properties (ln(AI)–ln(GI) and ln(AI)–ln($Vp$)).

Figure 7 displays the elastic properties predicted for the CMP gather located in correspondence of the blind well. In figure 7(a) note the clear class III AVA anomaly (according to Castagna and Swan 1997) at 2.45 s that characterizes the reservoir reflection. Figures 7(b)–(d) point out the good accordance between estimated and true properties. Note that we assume null initial models for $\delta$ln(GI) and $\delta$ln($Vp$), that correspond to initial models that exactly follow the linear relations of equations (6) and (7).

Figure 8 represents the comparison between true and predicted petrophysical properties for the blind well. Again, note that the predicted petrophysical curves show a close match with actual well log data. This blind test proves the applicability and the reliability of the implemented method for reservoir characterization in the investigated area.

We now describe the AI and GI values estimated by the implemented deterministic inversion within the yellow rectangle shown in figure 5. In figure 9 the low AI and GI values within the red rectangle identify the reservoir interval. Figure 10 shows the predicted petrophysical properties within the yellow rectangle shown in figure 5. Note the high porosity and low water saturation and shaliness values associated with the target interval, together with the complex geologic setting

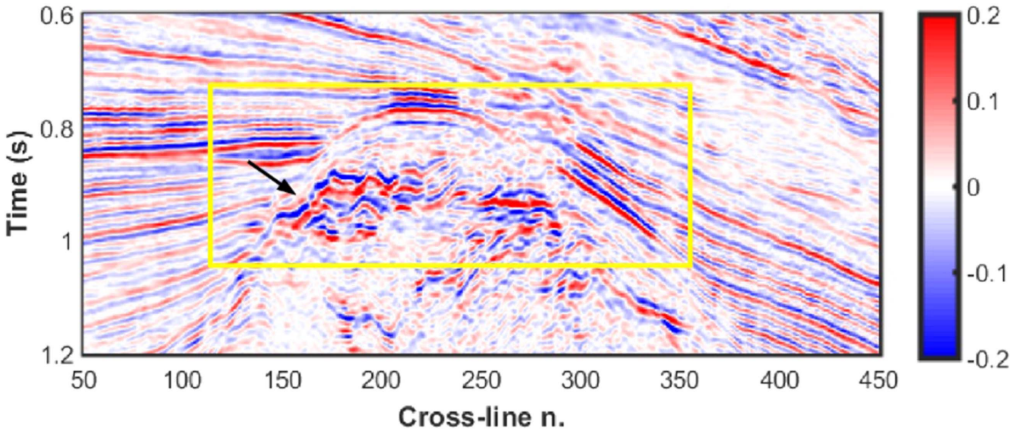


**Figure 13.** Example of stack section along an in-line direction extracted from the 3D seismic volume. The yellow rectangle delimits the target zone, while the black arrow points toward the top reflection of the reservoir.

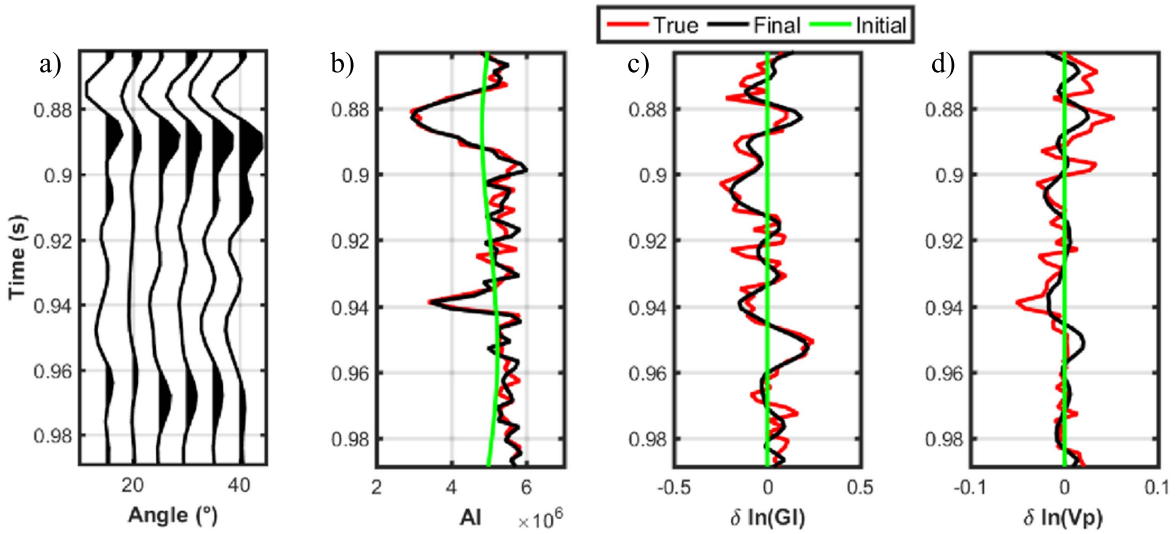


**Figure 14.** Inversion results for the seismic gather closest to the blind well. (a)–(d) Represent the seismic data, the acoustic impedance, the $\delta$ln (GI) and the $\delta$ln($Vp$), respectively. In (b)–(d) the red, green and black lines show the true, the initial and the final predicted models, respectively. The amplitude anomaly at 0.86 s identifies the reservoir layer.

of the investigated area characterized by many isolated and interconnected sand channels surrounded by thick shale sequences.

## Field case 2: reservoir characterization on on-shore seismic data

This second test concerns the application of the EEI method to a clastic, gas-saturated reservoir, located on-shore. The reservoir zone is constituted by gas-bearing sands at the depth range of 900–1000 m. The reservoir sand is rather clean with no cementation and low clay content; effective porosity ranges from 0% to 35%, while gas saturation usually varies between 0% and 80%. Borehole logs from 6 out of 7 wells provide elastic and petrophysical information needed to fully characterize the reservoir rocks in terms of $Vp$, $Vs$, density, effective porosity, water saturation and shaliness. Similarly, to the previous field test case, the seventh, remaining, well has been used for a blind test to validate the final predictions. More information about the rock-physics analysis for the investigated zone can be found in Aleardi *et al* (2018).

Figure 11 represents the rock-physics template for the investigated area in which the effects of water saturation, porosity and shaliness on the elastic properties of AI and GI are displayed. Again, we observe the decrease of GI and AI as the porosity increases and as the water saturation and shaliness decrease. We can also observe that even slight variations in the porosity exert a significant influence on the elastic properties, whereas the shaliness, but particularly the water saturation, play much minor roles in controlling the AI and GI values. For this reason, we expect that the predicted porosity will be affected by lower error than the estimated shaliness and the water saturation values. In other words, we are more confident on the porosity estimates than on the predicted water saturation values.

Figure 12 displays the EEI correlation graph for porosity, water saturation, and shaliness for the investigated reservoir. In this case, the porosity shows a strong negative correlation

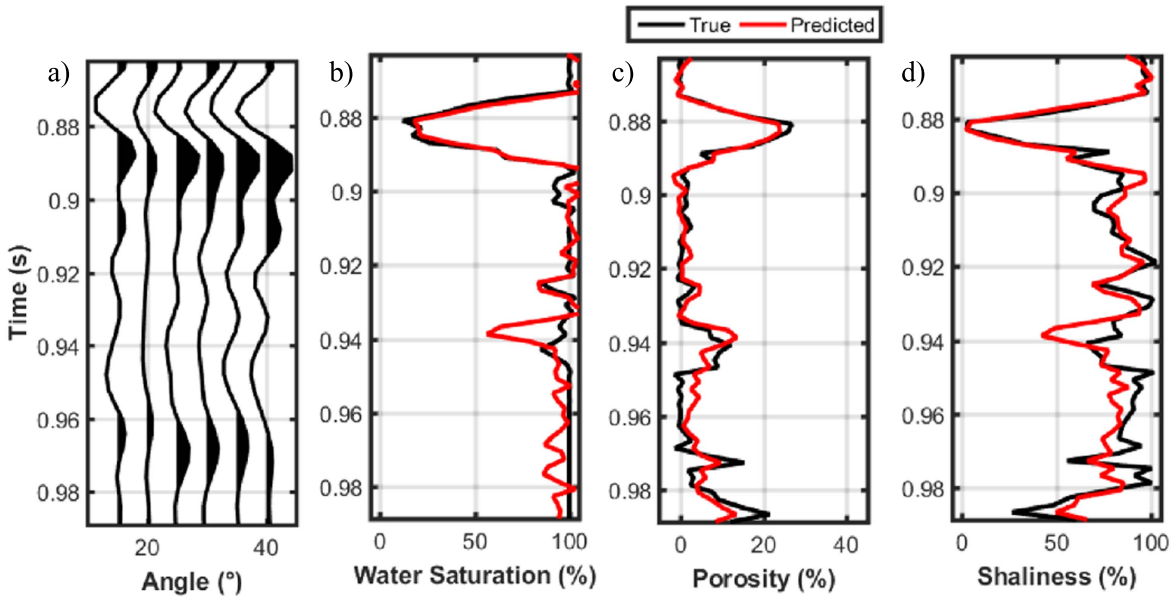


**Figure 15.** Petrophysical properties estimated for the seismic gather closest to the blind well. (a)–(d) Represent the seismic data, water saturation, porosity and shaliness, respectively. In (b)–(d) the black and red lines illustrate the true and the final predicted models, respectively.

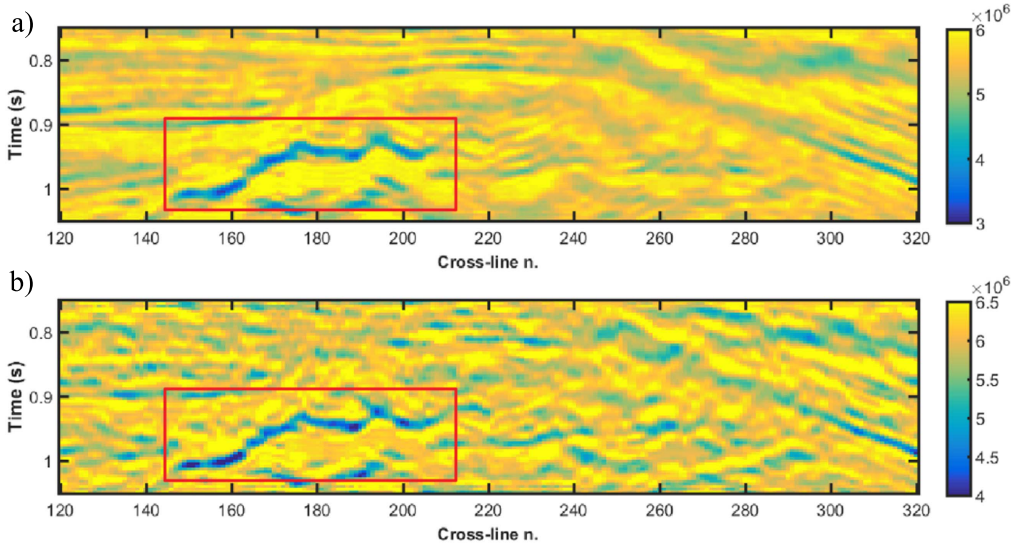


**Figure 16.** (a) and (b) Show the AI and GI values estimated within the yellow rectangle represented in figure 13. The red rectangles enclose the target reservoir characterized by low AI and GI values.

with EEI for a null $\chi$ angle. This means that AI correlates well with porosity. Differently, water saturation and shaliness show correlation maxima at $\chi$ angles of 32° and 40°, respectively. Note that all the considered petrophysical properties show correlation maxima around an absolute value of 0.8. This evidences that the EEI method can be a valuable tool for quantitative reservoir characterization in the investigated area.

Figure 13 shows a close-up of a stack section extracted from the 3D seismic volume along an in-line direction. Note the high amplitude reflector associated with the top of the reservoir (indicated by the black arrow). The yellow rectangle encloses the reservoir zone investigated by the following inversion.

Figure 14 represents the elastic properties predicted for the CMP gather closest to the blind well. In figure 14(a) at 0.86 s note the clear negative amplitude anomaly marking the transition from the overlying cap-rock to the underlying reservoir layer. Figures 14(b)–(d) illustrate the close match between the predicted elastic properties and the actual well log information.

The comparison between the true and predicted petrophysical properties for the blind well shows satisfactory predictions (figure 15), that is the predicted properties correctly capture the variability in the logs. Similarly to the previous field application, these results prove the applicability and the reliability of the implemented method for reservoir characterization in the investigated on-shore reservoir. Figure 15 shows that the error (that is the deviation from the actual petrophysical

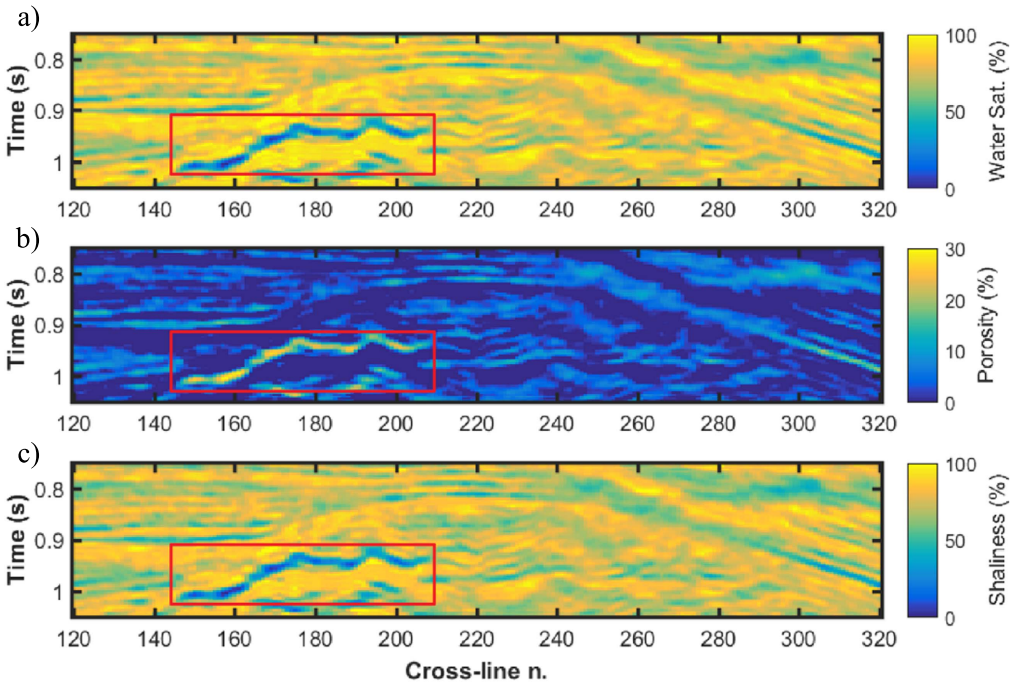


**Figure 17.** Petrophysical properties predicted within the yellow rectangle represented in figure 13. (a)–(c) Refer to water saturation, porosity and shaliness, respectively. Note the decreases of water saturation and shaliness and the increase of porosity occurring at the target zone, which is enclosed by the red rectangles.

property values) affecting the estimated parameters is higher for the shaliness, and particularly for the water saturation, whereas it is lower for the porosity, which shows a closer match with the actual well log information. This fact can be related to the minor role played by the shaliness, but particularly by the water saturation, in determining the elastic properties and then the seismic response.

Figure 16 displays the AI and GI values predicted within the yellow rectangle depicted in figure 13. As expected from the petrophysical analysis shown in figure 11, very low AI and GI values characterize the reservoir zone.

Finally, figure 17 illustrates the final predicted petrophysical properties for the target interval. Note the high porosity and low water saturation and shaliness values that characterize the reservoir zone.

## Conclusions

In this paper, we demonstrated the applicability of the EEI method for quantitative reservoir characterization in two different clastic reservoirs located on-shore and off-shore. In particular, we showed that EEI at specific $\chi$ angles is characterized by high correlation with the key reservoir properties of porosity, shaliness, and water saturation. The optimal $\chi$ angle for each reservoir property of interest should be established though appropriate rock-physics analysis of well log data. Once the $\chi$ angles are defined, the EEI volumes at estimated optimal $\chi$ angles can be generated from the AI and GI values derived through pre-stack AVA inversion. The so obtained EEI volumes can be considered appropriate information support for reservoir characterization. As EEI volumes have measurable high correlation with reservoir properties, they can be easily integrated as secondary information into the static reservoir model building to constrain properties in the inter-well regions. In addition, the estimated petrophysical volumes can be exploited to map favorable zones for future drilling locations. Obviously, for a successful application of the EEI method for reservoir characterization all the requirements for AVA analysis must be met. In particular, care should be taken during data processing and conditioning to ensure that the reservoir AVA responses are preserved in the seismic data.

We are aware that the present paper cannot prove the suitability of the EEI approach for reservoir characterization in all the possible geologic scenarios that can be encountered in hydrocarbon exploration. However, some conclusions we drew, although specifically valid for the analyzed cases, could reveal to be of practical utility in similar contexts (i.e. clastic reservoirs hosted in shale-sand sequences). In different geologic scenarios (i.e. non-clastic rocks, fractured rocks) the complex interrelationships between petrophysical and elastic parameters could make the EEI method inapplicable. In these cases, the prediction of petrophysical parameters from seismic data or elastic properties requires more sophisticated inversion strategies based on tailored rock-physics models.

## Acknowledgments

The author wishes to thank Edison for the permission to publish this work and Dr Fabio Ciabarri and Dr Timur Gukov of Edison for their continuous support to this research project. At the University of Pisa, the seismic data were processed with the Promax software of Landmark/Halliburton who is gratefully acknowledged.

## ORCID iDs

Mattia Aleardi https://orcid.org/0000-0003-1433-0281

## References


Aleardi M 2018 Applying a probabilistic seismic-petrophysical inversion and two different rock-physics models for reservoir characterization in offshore nile delta *J. Appl. Geophys.* **148** 272–86

Aleardi M and Ciabarri F 2017a Assessment of different approaches to rock-physics modeling: a case study from offshore nile delta *Geophysics* **82** MR15–25

Aleardi M and Ciabarri F 2017b Application of different classification methods for litho-fluid facies prediction: a case study from offshore nile delta *J. Geophys. Eng.* **14** 1087

Aleardi M, Ciabarri F and Gukov T 2018 A two-step inversion approach for seismic-reservoir characterization and a comparison with a single-loop markov-chain monte carlo algorithm *Geophysics* **83** R227–44

Aleardi M, Ciabarri F and Mazzotti A 2017 Probabilistic estimation of reservoir properties by means of wide-angle AVA inversion and a petrophysical reformulation of the zoeppritz equations *J. Appl. Geophys.* **147** 28–41

Avseth P, Mukerji T and Mavko G 2010 *Quantitative Seismic Interpretation: Applying Rock Physics Tools to Reduce Interpretation Risk* (Cambridge: Cambridge University Press)

Avseth P A, Veggeland T, Christiansen M, Ĺrdal K J and Horn F 2013 Pseudo-elastic impedance calibrated to rock physics models for efficient lithology and fluid mapping from AVO data *75th EAGE Conf. and Exhibition*

Bachrach R 2006 Joint estimation of porosity and saturation using stochastic rock-physics modeling *Geophysics* **71** O53–63

Ball V, Blangy J P, Schiott C and Chaveste A 2014 Relative rock physics *Leading Edge* **33** 276–86

Ball V, Blangy J P and Tenorio L 2013 Statistical aspects of rock property depth series: the trend is not your friend *SEG Technical Program Expanded Abstracts* vol 2013 (Society of Exploration Geophysicists) pp 2326–30

Buland A and Omre H 2003 Bayesian linearized AVO inversion *Geophysics* **68** 185–98

Castagna J P and Swan H W 1997 Principles of AVO crossplotting *Leading Edge* **16** 337–44

Chatterjee R, Gupta S D and Farroqui M Y 2013 Reservoir identification using full stack seismic inversion technique: a case study from Cambay basin oilfields, India *J. Pet. Sci. Eng.* **109** 87–95

Connolly P 1999 Elastic impedance *Leading Edge* **18** 438–52

Doyen P M 1988 Porosity from seismic data: a geostatistical approach *Geophysics* **53** 1263–75

Dubucq D, Busman S and Van Riel P 2001 Turbidite reservoir characterization: multi-offset stack inversion for reservoir delineation and porosity estimation; a Golf of Guinea example *SEG Technical Program Expanded Abstracts* vol 2001, pp 609–12

Grana D and Della Rossa E 2010 Probabilistic petrophysical-properties estimation integrating statistical rock physics with seismic inversion *Geophysics* **75** O21–37

Hampson D P, Russell B H and Bankhead B 2005 Simultaneous inversion of pre-stack seismic data *SEG Technical Program Expanded Abstracts* vol 2005, pp 1633–7

Samba C P, Lu H and Mukhtar H 2017 Reservoir properties prediction using extended elastic impedance: the case of nianga field of West African Congo basin *J. Pet. Explor. Prod. Technol.* **7** 673–86

Sams M, Millar I, Satriawan W, Saussus D and Bhattacharyya S 2011 Integration of geology and geophysics through geostatistical inversion: a case study *First Break* **29** 47–56

Sengupta M and Bachrach R 2007 Uncertainty in seismic-based pay volume estimation: analysis using rock physics and Bayesian statistics *Leading Edge* **26** 184–9

Shi L, Liu J, Dong N, Wang J and Xia H 2014 Extended elastic impedance inversion technology and its application of tight and thin reservoir *76th EAGE Conf. and Exhibition* vol 2014

Shuey R T 1985 A simplification of the Zoeppritz equations *Geophysics* **50** 609–14

Thomas M, Ball V, Blangy J P and Davids A 2013 Quantitative analysis aspects of the EEI correlation method *SEG Technical Program Expanded Abstracts* vol 2013, pp 2321–5

Vernik L, Fisher D and Bahret S 2002 Estimation of net-to-gross from P and S impedance in deepwater turbidites *Leading Edge* **21** 380–7

Whitcombe D N, Connolly P A, Reagan R L and Redshaw T C 2002 Extended elastic impedance for fluid and lithology prediction *Geophysics* **67** 63–7

Wiggins R, Kenny G S and McClure C D 1983 A method for determining and displaying the shear-velocity reflectivities of a geologic formation *European Patent Application* 83300227.2, Bull. 84/30